processes

Article

Power Flow Analysis of Ring AC/DC Hybrid Network with Multiple Power Electronic Transformers Based on Hybrid Alternating Iteration Power Flow Algorithm

Zhen Zheng [1], Chenhong Huang [1], Xiaoli Ma [1], Wenwen Chen [1], Yinan Huang [1], Min Wang [2,*] and Dongqian Pan [2,*]

[1] State Grid Shanghai Electric Power Company Qingpu Power Supply Company, Shanghai 201700, China; upczz@126.com (Z.Z.); huangch@sh.sgcc.com.cn (C.H.); ma_xl@sh.sgcc.com.cn (X.M.); chenwenwen@sh.sgcc.com.cn (W.C.); huangyn@sh.sgcc.com.cn (Y.H.)
[2] School of Electrical and Power Engineering, Hohai University, Nanjing 211100, China
* Correspondence: wangmin@hhu.edu.cn (M.W.); q15195953033@163.com (D.P.)

Abstract: AC/DC hybrid distribution networks with power electronic transformers (PETs) as distribution hubs are in line with the future development direction of the AC/DC hybrid distribution network. Unlike traditional transformers, power electronic transformers introduce new node types and may transform the network topology from radial to ring structures. These changes render traditional power flow calculation methods inadequate for achieving satisfactory results in AC/DC hybrid networks. In addition, existing commercial power flow calculation software packages are mainly based on the traditional AC power flow calculation method, which have limited support for the DC network. Especially when the DC network is coupled with the AC network, it is difficult to achieve a unified calculation of its power flow. To address these challenges, this paper proposes a novel power flow calculation method for ring AC/DC hybrid distribution networks with power electronic transformers. The proposed method is based on the alternating iterative method to ensure compatibility with mature AC power flow calculation programs in commercial software, thereby improving the feasibility of engineering applications. Firstly, the steady-state power flow calculation model of PET is constructed by analyzing that the working principle and control modes of power electronic transformer are proposed based on the source-load attributes of its connected subnetworks. According to the characteristics of the power electronic transformer, AC distribution network, and DC distribution network, a hybrid alternating iteration method combining the high computational accuracy of the Newton–Raphson (NR) method with the high efficiency of the Zbus Gaussian method in dealing with ring networks is proposed. On this basis, the power flow calculation model of the AC/DC hybrid distribution network with power electronic transformers is established. Finally, the simulation of the constructed 44-node ring AC/DC hybrid distribution network example is carried out. The simulation results show that the proposed method can not only converge reliably when the convergence accuracy is 1×10^{-6} p.u., but also ensure that the voltage magnitudes of all nodes are above 0.96 p.u. whose maximum offset value is 0.789% when the outputs of the connected distributed generations fluctuate, which verifies the effectiveness and accuracy of the proposed method.

Keywords: AC/DC hybrid distribution network; power electronic transformers; power flow calculation; hybrid alternating iteration algorithm

check for updates

Academic Editor: Hsin-Jang Shieh

Received: 5 November 2024
Revised: 13 December 2024
Accepted: 18 December 2024
Published: 24 December 2024

Citation: Zheng, Z.; Huang, C.; Ma, X.; Chen, W.; Huang, Y.; Wang, M.; Pan, D. Power Flow Analysis of Ring AC/DC Hybrid Network with Multiple Power Electronic Transformers Based on Hybrid Alternating Iteration Power Flow Algorithm. *Processes* **2025**, *13*, 7. https://doi.org/10.3390/pr13010007

1. Introduction

Compared with the traditional AC power system, the DC power system is more convenient for distributed generation (DG) integration, which can effectively reduce transmission losses, and the DC load integration has fewer phase change links, lower fault rate, less difficult control, and higher reliability. However, the main power loads in the power system are still AC equipment, so the grid-connected operation of DC equipment will lead to a mixed operation of AC and DC loads in the long-term distribution network in the future. The AC/DC hybrid distribution network has the advantage of flexible use of AC and DC energy, and has become the main trend of distribution network development under the new power system in the future.

The development and evolution of AC/DC hybrid distribution networks went through three stages [1]: traditional AC distribution networks without a DC bus [2], AC/DC hybrid distribution networks with bidirectional converters [3–6], and AC/DC hybrid distribution networks with power electronic transformers (PETs) [7–9]. The first stage is shown in Figure 1, where each distributed renewable energy generation link is mainly connected to the AC distribution network through its own AC and DC conversion equipment, which directly limits the full consumption and efficient use of distributed renewable energy. The reason is that on the one hand, with the current renewable energy more access to the AC distribution network, AC/DC conversion links are more, reducing the efficiency and affecting the convenience of access; on the other hand, the distribution network interconnection and mutual aid and flexible regulation and control capacity is insufficient but also limits the capacity to integrate electricity generated from renewable energy sources and efficient use of distributed renewable energy.

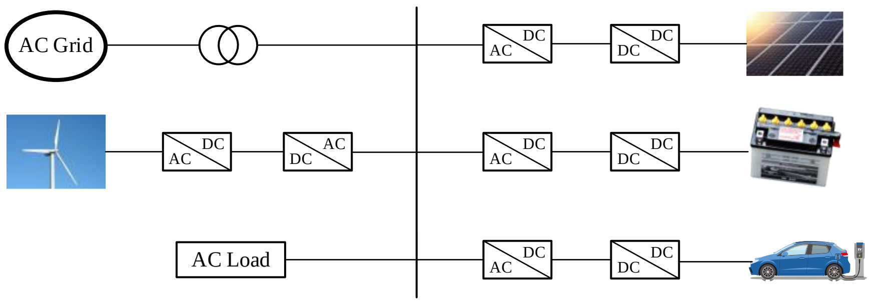

Figure 1. Traditional AC distribution networks without DC bus.

To solve the above problems, the development of an AC/DC hybrid distribution network entered into the second stage, as shown in Figure 2, where DC-type DGs such as photovoltaics (PVs) and DC loads such as electric vehicles are united to access the original AC grid through non-isolated bidirectional converters [5,6] to reduce AC/DC conversion links and improve the utilization efficiency. The non-isolated bi-directional converter often adopts a simple non-isolated AC/DC topology, which can only realize the interconnection of an AC sub-network and a DC sub-network, with a single form of networking. Meanwhile, the lack of transformer function of the non-isolated bi-directional converter makes it necessary to match the voltage level of the interconnected sub-networks, which restricts the flexibility of the power grid interconnection. Moreover, the non-isolated bi-directional converter also has the defects of lower voltage level and smaller capacity, so it is only suitable for low-voltage small-capacity microgrid interconnection, and its capacity to integrate electricity generated from renewable energy sources remains limited [10].

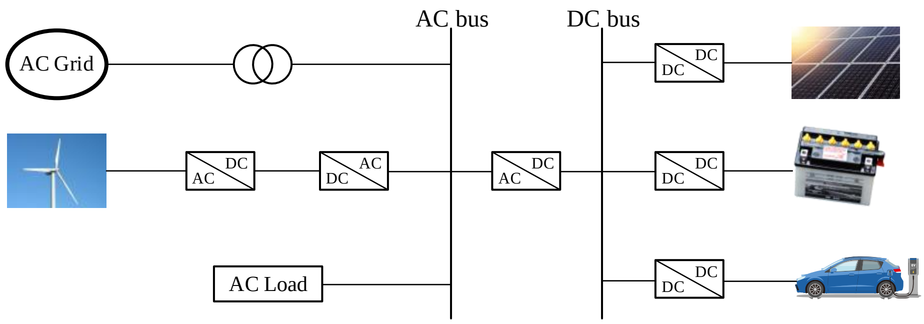

Figure 2. AC/DC hybrid distribution networks with non-isolated bidirectional converters.

The third stage of evolution is an AC/DC hybrid distribution network with PETs, as shown in Figure 3. PET consists of power electronic converters and high-frequency transformers with voltage conversion, electrical isolation, and energy transmission functions, which can realize the flexible networking of multiple AC/DC networks at multiple voltage levels, and interconnect and complement each other on a wider scale to realize the full consumption and high efficiency of renewable energy sources [11]. The multi-level converter structure of PET provides multiple interconnection ports, which makes the AC/DC distribution system more flexible in terms of network formation, operation mode, and coordination control. Reference [7] proposes a scheme to interconnect AC and DC grids by using PET as an energy control center. Reference [8] classifies the AC/DC hybrid system in which the PET is located into two modes, on-grid and off-grid, and uses different operation strategies for optimization depending on the mode of operation.

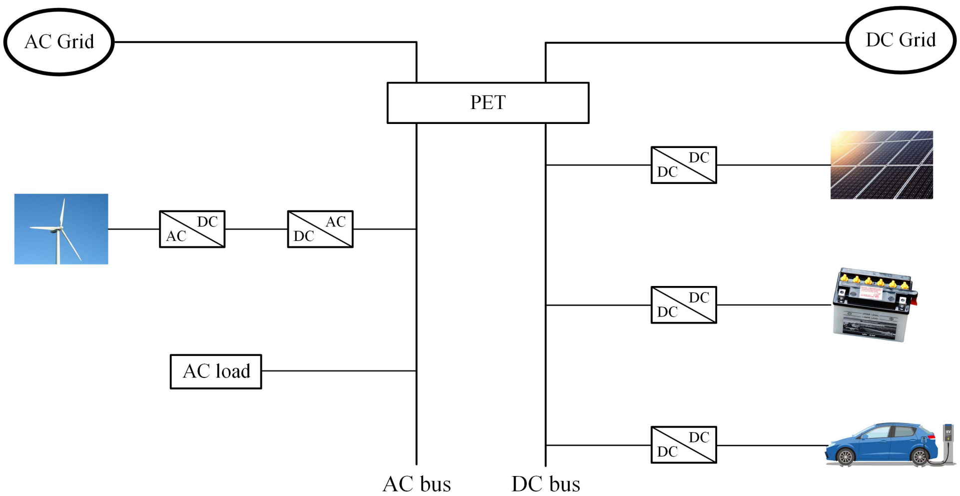

Figure 3. AC/DC hybrid distribution networks with PETs.

Obviously, the AC/DC hybrid distribution network shown in Figures 2 and 3 is different from the traditional AC distribution network without the DC bus shown in Figure 1 in terms of transformer type, network structure, and operation mode. Therefore, the traditional power flow calculation methods cannot be applied to the AC/DC hybrid distribution network, so it is necessary to establish a brand new system model for analyzing and solving power flow. The existing power flow calculation methods of AC/DC hybrid distribution networks are mainly divided into two categories: unified solution method [12–15] and alternating iterative method [16–18]. The unified solution method jointly solves the AC system equation and the DC system equation. The alternating solution method solves the DC system power flow equation and the AC system power flow equation separately and iterates alternately until convergence.

The unified solution method can fully reflect the relationship between AC and DC sub-networks. When solving a small-scale AC/DC hybrid distribution network, it has good convergence performance and secondary iteration accuracy [12]. However, in a large-scale AC/DC hybrid distribution network, the distribution network has many nodes and complex structure. The dimension of the Jacobian matrix to be solved increases, which will increase the amount of calculation and reduce the calculation rate. Reference [13] proposed an AC/DC unified power flow model in augmented rectangular coordinates. Compared with the traditional polar coordinates or rectangular coordinates, the Jacobian matrix is sparser, and most of the non-zero elements remain constant during the iteration process, which greatly improves the efficiency of power flow calculation, but the amount of computation is still large. Reference [14] integrated the AC system and the DC system matrix by using the extended matrix method and solved it by the unified iterative method, which simplified the calculation. Reference [15] obtained a sparse Jacobian matrix by classifying the mismatch equations and then proposed a generalized unified power flow algorithm for AC/DC hybrid power grids with voltage source converters (VSCs) suitable for any topology and different DC voltage control modes. The algorithm can correct the reference value by the constrained power flow method even if the obtained solution is infeasible or divergent, so as to obtain the feasible solution automatically.

The alternating iterative method can effectively reduce the dimension of the equation. It is easy to program and has scalability and flexibility. However, this method only transmits the interaction between the AC and DC sub-networks through the common connection point, and the coupling is poor. The number of iterations may increase significantly or not converge. Reference [16] proposes an alternating tidal current iterative algorithm for hybrid AC/DC distribution networks that can be applied to different control modes and arbitrary topologies, but the algorithm can only roughly take into account the corrected direction of the DC network after overrunning the limit, and it cannot guarantee that the system must be able to find a feasible solution. Reference [17] proposes an AC/DC decoupled hybrid tidal current algorithm containing VSC, which is improved on the basis of the alternating iteration method by changing the division boundary of AC subsystems and DC subsystems from the common connection point to the AC outlet of the VSC, and changing the alternating computation repeated many times to a single alternating computation so that the convergence and efficiency of the algorithm are improved. Reference [18] establishes the power flow model for AC/DC networks and proposes the dynamic power flow alternating iteration algorithm suitable for AC/DC hybrid networks with VSCs using virtual synchronous machine control. The VSC injected power and the voltage of each DC node derived by the dynamic power flow algorithm is more accurate. However, if there are multiple VSCs in the system, the number of nodes to be calculated will increase, so that the calculation results are not easy to converge.

All of the above studies focus on AC/DC hybrid networks containing VSCs, and compared with VSCs, electrical ports of PET can be connected to different types of power supply, energy storage, and load equipment, which can not only realize the two-way flow of electric energy, but also have the real-time adjustment ability of voltage or current power [19]. Therefore, the original power flow calculation method for the AC/DC hybrid distribution network can no longer be applied to the analysis and calculation of AC/DC hybrid distribution networks containing PETs. Reference [20] proposes a steady-state power flow computation model for a PET-based multiport energy router based on VSC. Reference [21] establishes a three-port PET equivalent model based on the power balance relationship of the DC/DC converter link, combined with the dynamic and static power loss estimates of the transformer, which did not solve the coupling problems of the DC ports and the AC/DC side, although the internal topology of the PET was considered. Reference [22] fully considers the coupling relationship between the ports of PET, establishes a more accurate equivalent model for power flow calculation of PET, and proposes an AC/DC decoupled iterative power flow algorithm for PET-containing distribution networks based on reference [17], but it could not realize the power flow calculation for the AC/DC hybrid distribution network containing PET based on ring topology.

In this regard, this paper proposes a hybrid alternating iterative power flow calculation method combining the Newton–Raphson (NR) method and Zbus Gaussian method. First of all, a steady-state model of PET is established, and control modes of PET are proposed. Secondly, the power flow calculation model of the PET AC power grid is established by the NR method, and the power flow calculation model of the DC power grid is established by the Zbus Gaussian method. Then, based on the control scheme for multiple PETs in the AC/DC hybrid distribution network, an AC/DC hybrid alternating iterative power flow algorithm is proposed. Finally, an example of an improved IEEE 33-bus system connected to the DC system is constructed. The example analysis of the distribution network test system verifies the effectiveness and accuracy of the proposed algorithm and the power flow regulation ability of PET in the system.

The contributions of this paper are summarized as follows:

(1) We propose a hybrid alternating iteration power flow algorithm for a ring AC/DC hybrid network with multiple PETs, which has not been studied.
(2) The hybrid alternating iteration power flow algorithm not only retains the advantages of the NR method in terms of high computational accuracy and good convergence, but also makes full use of the superiorities of the Zbus Gaussian method in terms of its high computational speed and its specialty in dealing with the ring distribution network.
(3) Ability of PETs to effectively reduce the impact of the output mutation of DGs on power systems and good convergence performance of the proposed power flow method for ring AC/DC hybrid distribution networks are demonstrated by performing power flow calculations on the constructed 44-node example under different output scenarios of DGs.

2. Steady-State Model and Control Modes of PET

2.1. Working Principle of PET

PET is a new type of substation device using a power electronic converter (rectifier and inverter) combined with a high-frequency transformer (HFT), which has the functions of realizing power conversion, energy transmission, and improving power quality. The working principle of PET is as follows: the input power frequency electric energy is transformed by the power electronic converter, and the power frequency signal is raised to a high-frequency square wave signal. The high-frequency square wave signal passes through the primary winding of HFT, is magnetically coupled to the secondary winding according to the principle of electromagnetic induction, and then transmitted to the power electronic converter on the PET output side.

The multiport PET can be divided into three parts, which are the input port based on VSC, the isolation module based on a dual-active bridge (DAB) DC/DC converter, and the output port based on a VSC or DC/DC converter which depends on the type of grid connected [23]. The physical structure of PET is shown in Figure 4.

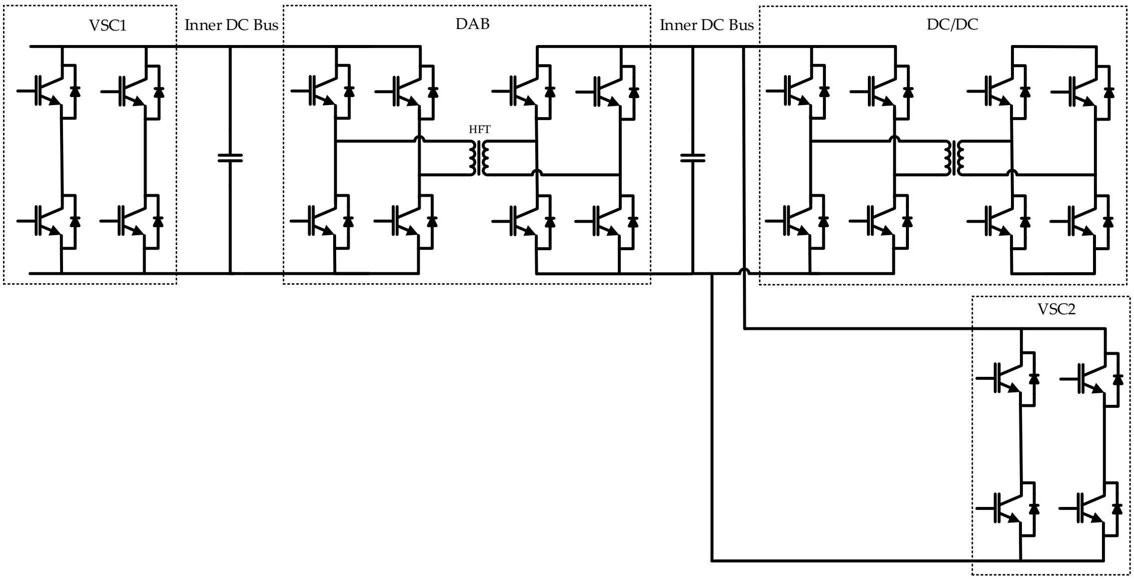

Figure 4. Physical structure of PET.

According to Figure 4, PET has a complex structure and a large number of power electronic devices. Due to its many transformation links, PET can achieve a variety of control functions and flexibly control the waveforms of voltage, current, and power on the primary and secondary sides, which can be applied to a variety of occasions. Moreover, the primary and secondary sides can be cascaded by multiple modules, so as to improve the voltage level and capacity level.

2.2. Steady-State Model of PET

As outlined in Section 2.1, there are two distinct types of ports in PET: AC ports based on VSCs and DC ports based on DC/DC converters. These two types of ports will be thoroughly analyzed and modeled separately in the following sections. Additionally, the power of each port of the PET needs to be coordinated by an internal isolated DC/DC converter, and therefore an internal power conservation model is also required.

2.2.1. AC Port Modeling of PET

The steady-state model of the AC port of PET is shown in Figure 5. G and B represent equivalent conductance and equivalent susceptance considering VSC loss, respectively. U_{ac}^{s} represents the voltage magnitude of the AC grid node to which the VSC is connected. U_{ac}^{w} represents the modulation voltage magnitude on the AC side of the VSC. θ_{ac}^{s} represents the phase angle of the AC grid node to which the VSC is connected. θ_{ac}^{w} represents the modulation angle on the AC side of the VSC. U_d is the inner DC bus voltage of PET. P_{ac}^{s} and Q_{ac}^{s} represent the active and reactive power exchanged between the VSC and the connected AC grid node, respectively. P_{ac}^{w} and Q_{ac}^{w} represent the active and reactive power absorbed by VSC, respectively.

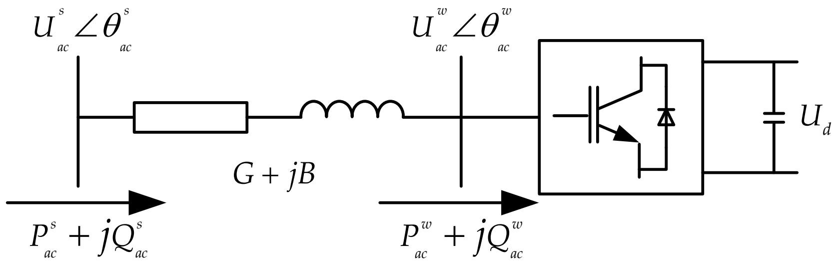

Figure 5. Model of the AC port based on VSC.

The VSC-based AC port steady-state model is constructed as follows:

$$\begin{cases} P^s_{ac} = G(U^s_{ac})^2 - U^s_{ac}U^w_{ac}(G\cos\theta_{VSC} + B\sin\theta_{VSC}) \\ Q^s_{ac} = -B(U^s_{ac})^2 + U^s_{ac}U^w_{ac}(B\cos\theta_{VSC} - G\sin\theta_{VSC}) \\ P^w_{ac} = -G(U^w_{ac})^2 + U^s_{ac}U^w_{ac}(G\cos\theta_{VSC} + B\sin\theta_{VSC}) \\ Q^w_{ac} = B(U^w_{ac})^2 - U^s_{ac}U^w_{ac}(B\cos\theta_{VSC} - G\sin\theta_{VSC}) \end{cases} \quad (1)$$

where θ_{VSC} represents the angle by which U^w_{ac} lags U^s_{ac}.

The relationship between U^w_{ac} and U_d can be expressed as follows:

$$U^w_{ac} = \frac{\mu m}{\sqrt{2}}U_d \quad (2)$$

where μ represents the DC voltage utilization rate, and m represents the modulation ratio ($0 < m < 1$). In this paper, it is assumed that VSC adopts a pulse width modulation (PWM) mode with $\mu = 1$.

2.2.2. DC Port Modeling of PET

The steady-state model of the DC port of PET is shown in Figure 6. r represents the equivalent resistance of DC port power loss and q represents the ratio of the input stage to the output stage of the converter. U^s_{dc} represents the voltage of the input stage of the converter. U^d_{dc} represents the voltage of the output stage of the converter. U^s_{dc} represents the voltage of the input stage of the converter. I^s_{dc} represents the current of the input stage of the converter. I^d_{dc} represents the current of the output stage of the converter. P^s_{dc} represents the power of the input stage of the converter. P^d_{dc} represents the power of the output stage of the converter.

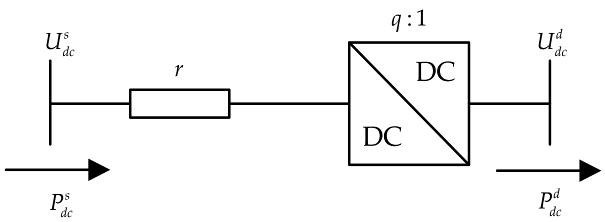

Figure 6. Model of the DC port based on the DC/DC converter.

The DC port steady-state model based on DC/DC converter is constructed as follows:

$$P^d_{dc} = P^s_{dc} - r(I^s_{dc})^2 \quad (3)$$

$$I^d_{dc} = \frac{1}{q}I^s_{dc} \quad (4)$$

$$U^s_{dc} = qU^d_{dc} \quad (5)$$

The objects connected to the input and output stages of the DC/DC converter change according to the different functions of the DC/DC converter. When the DC/DC converter plays the role of intermediate isolation, the input and output stage are connected to the inner DC bus of the corresponding side. The external network buses of PET are connected to the inner DC bus of PET, so the inner DC bus is used for power regulation and energy exchange. When the DC/DC converter is used as a DC port, the input stage is connected to the DC distribution grid outside the system, and the output stage is connected to the inner DC bus. The need for a DC/DC converter can be eliminated when the external DC distribution network and the inner DC bus are at the same voltage level and there are no stringent power control requirements for the port.

2.2.3. Internal Power Conservation Model of PET

In the distribution network, multiple VSCs and DC/DC converters form mutually independent external interfaces of the PET, and the total power of each port on the primary and secondary sides is converged at the inner DC bus on the corresponding side, and the buses on both sides are coordinately connected by the intermediate isolated DC/DC converter. The expression of power conservation inside the intermediate isolated DC/DC converter is as follows:

$$\sum_{k=1}^{M} P_{k,VSC} + \sum_{k=1}^{N} P_{k,DC/DC} - P_{loss} = 0 \tag{6}$$

where M is the number of AC ports of PET, N is the number of DC ports of PET, $P_{k,VSC}$ represents the active power flowing into the inner DC bus from the kth VSC used as the AC port of PET, $P_{k,DC/DC}$ represents the active power flowing into the inner DC bus from the kth DC/DC converters used as the DC port of PET, and P_{loss} represents the static loss of a DC/DC converter with intermediate isolation.

2.3. Control Modes of PET

The control mode of PET has an impact on both its node equivalence approach in the power flow calculation and the role it plays in the power flow control, and the control function of PET is mainly realized by the joint control of AC and DC ports. Meanwhile, the source-load properties of the network connected to the AC and DC ports of PET affect the control mode of the corresponding ports. In accordance with whether the network contains an adjustable power source that balances the power of the network, a network that contains a balancing node with adjustable power can be referred to as an active network, and a network that does not contain a balancing node with adjustable power can be referred to as a passive network. Due to the uncertainty of renewable energy output, it does not have the controllability of balancing the power of the network, so the network that contains only renewable energy sources but no other adjustable power sources is also passive. Then, the whole system can be divided into AC active and passive networks, as well as DC active and passive networks according to the adjustable characteristics. Table 1 demonstrates the corresponding control methods of the AC and DC ports of PET.

Table 1. Control modes of multi-port PET.

Port Type	Control Mode	Characteristic of Network
AC port	Mode 1 : Constant P_{ac}^{s} and Q_{ac}^{s}	AC active network
	Mode 2 : Constant U_{d} and Q_{ac}^{s}	AC active network
	Mode 3 : Constant U_{ac}^{s} and θ_{ac}^{s}	AC passive network

Table 1. *Cont.*

Port Type	Control Mode	Characteristic of Network
DC port	Mode 4 : Constant P_{dc}^{s}	DC active network
	Mode 5 : Constant U_{dc}^{s}	DC passive network
	Mode 6: Droop control	DC passive network

The equations corresponding to each of the above control modes are shown below.

(1) Mode 1: Constant P_{ac}^{s} and Q_{ac}^{s}

In Mode 1, the active power P_{ac}^{s} and reactive power Q_{ac}^{s} exchanged between the AC port and the connected AC grid remain constant. The corresponding control equation is expressed as follows:

$$\begin{cases} P_{ac}^{s} = P_{ac}^{s,ref} \\ Q_{ac}^{s} = Q_{ac}^{s,ref} \end{cases} \tag{7}$$

where $P_{ac}^{s,ref}$ and $Q_{ac}^{s,ref}$ are the set values of the active and reactive power exchanged between the AC port and the connected AC node, respectively.

(2) Mode 2: Constant Q_{ac}^{s} and U_{d}

In Mode 2, the reactive power Q_{ac}^{s} exchanged between the AC port and the connected AC grid and the inner DC bus voltage U_{d} of PET remain constant, which can balance the internal active power of PET. The corresponding control equation is expressed as follows:

$$\begin{cases} Q_{ac}^{s} = Q_{ac}^{s,ref} \\ U_{d} = U_{d}^{ref} \end{cases} \tag{8}$$

where U_{d}^{ref} is the set value of the voltage on the DC side of the VSC.

(3) Mode 3: Constant U_{ac}^{s} and θ_{ac}^{s}

In Mode 3, the voltage magnitude U_{ac}^{s} and the phase angle θ_{ac}^{s} of the AC node connected to the AC port remain constant, which can bear the responsibility of balancing the power of the connected AC gird. The corresponding control equation is expressed as follows:

$$\begin{cases} U_{ac}^{s} = U_{ac}^{s,ref} \\ \theta_{ac}^{s} = \theta_{ac}^{s,ref} \end{cases} \tag{9}$$

where $U_{ac}^{s,ref}$ and $\theta_{ac}^{s,ref}$ are the set values of the voltage and phase angle of the AC node to which the AC port is connected.

(4) Mode 4: Constant P_{dc}^{s}

In Mode 4, the DC power P_{dc}^{s} exchanged between the DC port and the connected DC grid remain constant. The corresponding control equation is expressed as follows:

$$P_{dc}^{s} = P_{dc}^{s,ref} \tag{10}$$

where $P_{dc}^{s,ref}$ is the set value of the active power exchanged between the DC port and the connected DC grid.

(5) Mode 5: Constant U_{dc}^{s}

In Mode 5, the voltage U_{ac}^{s} of the DC grid node connected to the DC port remains constant, which can bear the responsibility of balancing the power of the connected DC gird. The corresponding control equation is expressed as follows:

$$U_{dc}^{s} = U_{dc}^{s,ref} \tag{11}$$

where $U_{dc}^{s,ref}$ is the set value of the voltage of the DC node to which the DC port is connected.

(6) Mode 6: Droop control

In Mode 6, a linear relationship exists between the DC power P_{dc}^{s} exchanged between the DC port and the connected DC grid and the DC voltage U_{dc}^{s} of the DC port, which can realize the automatic coordination of $U_{dc}^{s,ref}$ and the automatic distribution of $P_{dc}^{s,ref}$. The corresponding control equation is expressed as follows:

$$P_{dc}^{s} = \frac{1}{k_{dp}^{s}}(U_{dc}^{s} - U_{dc}^{s,ref}) + P_{dc}^{s,ref} \tag{12}$$

where k_{dp}^{s} represents the droop coefficient of the DC port.

The droop coefficient can be selected according to the following formula:

$$k_{dp}^{s} = \frac{U_{dc}^{s,ref} - U_{dc}^{\max}}{P_{dc}^{s,ref} - P_{dc}^{\max}} \tag{13}$$

where $U_{dc}^{\max}$ is the maximum value of the voltage of connected DC grid, $P_{dc}^{\max}$ is the maximum value of the power exchanged between the DC port and the connected DC grid.

3. Power Flow Calculation Model for AC/DC Hybrid Distribution Network with Multiple PETs

To facilitate the use of a mature AC power flow calculation program in commercial software, this paper uses an alternating iterative method to calculate the power flow of an AC/DC hybrid distribution network with PETs.

The traditional power flow calculation methods of an AC distribution network include the forward and backward substitution (FBS) method, and the Zbus Gaussian method. Compared with the NR method, Zbus Gaussian method is simpler in principle, and easier in programming, and its derivative matrix is a sparse constant value matrix, which requires less computation in each iteration. Meanwhile, the Zbus Gaussian method has a greater advantage than the FBS method in solving the ring network, and has the convergence speed and convergence characteristics close to the NR method [24].

The NR method is adopted to calculate the power flow of the AC network due to its fast convergence and high accuracy in solving the nonlinear equations. In contrast, the DC network is a purely resistive linear network that transmits only active power, whose mathematical model is a set of linear equations. Consequently, the Zbus Gaussian method is adopted to calculate the power flow of the DC network, which ensures computational simplicity and efficiency. Therefore, this paper proposes an AC/DC hybrid alternating iterative power flow algorithm combining the NR method and the Zbus Gaussian method. The proposed algorithm combines the high accuracy of the NR method and the high efficiency of the Zbus Gaussian method, which is particularly suitable for ring AC/DC hybrid networks with multiple PETs, and fills in the shortcomings of existing methods in such scenarios.

3.1. Power Flow Calculation Model of Multiple PETs

The NR method is used to solve the power flow of PET with state variables m and θ_{VSC}. Usually, the AC port is set to the power balance port of PET. Assuming that there are z PETs in the network, the power flow equation for the i-th PET can be derived from Equations (1) and (2) as follows:

$$\begin{cases} P^s_{ac,i} = G_i[(U^s_{ac,i})^2 - \frac{m_i}{\sqrt{2}} U^s_{ac,i} U_{d,i} \cos\theta_{VSC,i}] + \frac{m_i}{\sqrt{2}} B_i U^s_{ac,i} U_{d,i} \sin\theta_{VSC,i} \\ Q^s_{ac,i} = B_i[-(U^s_{ac,i})^2 + \frac{m_i}{\sqrt{2}} U^s_{ac,i} U_{d,i} \cos\theta_{VSC,i}] - \frac{m_i}{\sqrt{2}} G_i U^s_{ac,i} U_{d,i} \sin\theta_{VSC,i} \end{cases}. \tag{14}$$

Then the power deviation equation of i-th PET is as follows:

$$\begin{cases} \Delta P^s_{ac,i} = P^{s,ref}_{ac,i} - \left\{ G_i[(U^s_{ac,i})^2 - \frac{m_i}{\sqrt{2}} U^s_{ac,i} U_{d,i} \cos\theta_{VSC,i}] + \frac{m_i}{\sqrt{2}} B_i U^s_{ac,i} U_{d,i} \sin\theta_{VSC,i} \right\} \\ \Delta Q^s_{ac,i} = Q^{s,ref}_{ac,i} - \left\{ B_i[-(U^s_{ac,i})^2 + \frac{m_i}{\sqrt{2}} U^s_{ac,i} U_{d,i} \cos\theta_{VSC,i}] - \frac{m_i}{\sqrt{2}} G_i U^s_{ac,i} U_{d,i} \sin\theta_{VSC,i} \right\} \end{cases} \tag{15}$$

where $\Delta P^s_{ac,i}$ and $\Delta Q^s_{ac,i}$ represent the power error of the active and reactive power at the AC port of i_{th} PET, and $P^{s,ref}_{ac,i}$ and $Q^{s,ref}_{ac,i}$ are the set values of the active and reactive power at the AC port of i-th PET.

3.2. Power Flow Calculation Model of AC Network

NR method is used to solve the power flow of the AC distribution network with state variable node voltage U_{ac} and node phase angle θ_{ac}. For an AC network with n nodes, the power flow equation of the AC network is as follows:

$$\begin{cases} P_{ac,i} = U_{ac,i} \sum\limits_{j=1}^{n} U_{ac,j}(G_{ij} cos\theta_{ac,ij} + B_{ij} sin\theta_{ac,ij}) \\ Q_{ac,i} = U_{ac,i} \sum\limits_{j=1}^{n} U_{ac,j}(G_{ij} sin\theta_{ac,ij} - B_{ij} cos\theta_{ac,ij}) \end{cases} \tag{16}$$

where $P_{ac,i}$ and $Q_{ac,i}$ are the injected active power and reactive power of node i in the AC network, respectively, $U_{ac,i}$ and $U_{ac,j}$ represent the voltage magnitude of nodes i and j in the AC network, respectively, G_{ij} and B_{ij} represent the conductance and susceptance between nodes i and j in the AC network, respectively, and $\theta_{ac,ij}$ represents the phase angle difference between nodes i and j in the AC network, respectively.

Then the power deviation equation of the AC network is as follows:

$$\begin{cases} \Delta P_{ac,i} = P_{aci,0} - U_{ac,i} \sum\limits_{j=1}^{n} U_{ac,j}(G_{ij} cos\theta_{ac,ij} + B_{ij} sin\theta_{ac,ij}) \\ \Delta Q_{ac,i} = Q_{aci,0} - U_{ac,i} \sum\limits_{j=1}^{n} U_{ac,j}(G_{ij} sin\theta_{ac,ij} - B_{ij} cos\theta_{ac,ij}) \end{cases} \tag{17}$$

where $\Delta P_{ac.i}$ and $\Delta Q_{ac.i}$ represent the active and reactive power error of node i in the AC network, and $P_{aci,0}$ and $Q_{aci,0}$ are given active and reactive power of node i in the AC network.

3.3. Power Flow Calculation Model of DC Network

The Zbus Gaussian method is used to solve the power flow of the DC distribution network with state variable node voltage U_{dc}. The power flow equation of the DC network is as follows:

$$\boldsymbol{I}_{dc} = \boldsymbol{Y}_{dc} \boldsymbol{U}_{dc} \tag{18}$$

where $\boldsymbol{U}_{dc}$ is the DC node voltage matrix; $\boldsymbol{I}_{dc}$ is the DC node injection current matrix; and $\boldsymbol{Y}_{dc}$ is the node admittance matrix of DC distribution network.

The balance node of DC distribution system is separated from other nodes, and the system equation can be written as follows:

$$\begin{bmatrix} \boldsymbol{I}_{dc,1} \\ \boldsymbol{I}_{dc,2} \end{bmatrix} = \begin{bmatrix} \boldsymbol{Y}_{dc,11} \boldsymbol{Y}_{dc,12} \\ \boldsymbol{Y}_{dc,21} \boldsymbol{Y}_{dc,22} \end{bmatrix} \begin{bmatrix} \boldsymbol{U}_{dc,1} \\ \boldsymbol{U}_{dc,2} \end{bmatrix} \tag{19}$$

where $\boldsymbol{I}_{dc,1}$ and $\boldsymbol{U}_{dc,1}$ represent the current and voltage vectors of the source node, and $\boldsymbol{I}_{dc,2}$ and $\boldsymbol{U}_{dc,2}$ represent the current and voltage vectors of the other nodes except the balance node.

For a DC network with g nodes, the injection power of the i-th DC node is as follows:

$$P_{dc,i} = \sum_{i=1}^{g} \sum_{j=1}^{g} U_{dc,i} U_{dc,j} Y_{ij} \tag{20}$$

where $P_{dc,i}$ represents the injected active power of node i in the DC distribution network, $U_{dc,i}$ and $U_{dc,j}$ represent the voltage magnitude of nodes i and j in the DC distribution network, and Y_{ij} represents the element of the i-th row and j-th column of $\boldsymbol{Y}_{dc}$.

4. AC/DC Hybrid Alternating Iterative Power Flow Algorithm

4.1. Control Scheme for Multiple PETs in the AC/DC Hybrid Distribution Network

When the AC/DC hybrid distribution network with multiple PETs is divided into multiple sub-systems, a passive AC system may occur. The passive AC system is characterized by the absence of adjustable power sources that balance the power of the network, thus the AC port of the PET to which it is connected must operate in constant U_{ac}^s and θ_{ac}^s control mode, which takes responsibility for balancing the power of the network. The AC port of the PET connected to the active AC system can operate in constant P_{ac}^s and Q_{ac}^s control mode or constant Q_{ac}^s and U_d control mode, whereas one side of the AC or DC port must be left as a slack port which operates in constant Q_{ac}^s and U_d control mode to maintain the active power balance within the PET. The DC port of PET is an active power exchange port based on the DC/DC converter. The DC system has only two types of nodes, which are power point and voltage point, respectively. For the inner DC bus of PET, each DC port is considered a power point with known active power, and the node type of the DC system depends on the control mode of the DC port. When the DC port does not operate in constant P_{dc}^s control mode, the connected DC node type needs to be adjusted to a voltage point which operates in constant U_{dc}^s control mode.

4.2. Solution Step

This paper proposes an AC/DC hybrid alternating iterative power flow algorithm. The specific solution steps are as follows:

(1) Initialize all the original data of the system, including the parameters related to the generator units, distributed power sources, branches, nodes, loads, and PETs of the AC/DC distribution network.

(2) Partition the system with the ports of PETs as boundaries. The AC/DC hybrid distribution system is divided into several AC subsystems and DC subsystems.

(3) Determine control modes and control parameters for all ports of PETs according to Table 1.

(4) Calculate the power flow of each subsystem which is not connected to the slack port of PET. If the power flow calculation converges, continue step (5); otherwise, return step (3).

(5) Obtain the injected power on the non-slack port side. If the direction of injection of PET is specified as the positive direction of power, the exchange power of the PET port P_T is equivalent to the difference between the output power P_s and the original power P_{load} of the connected node.

$$P_T = P_s - P_{load} \tag{21}$$

(6) Solve the equation for the power flow inside PET to obtain the injected power on the slack port side. The calculation formulas are as follows:

$$P^w_{ac,l} = P^{s,ref}_{ac,l} - \frac{P^{s,ref2}_{ac,l} + Q^{s,ref2}_{ac,l}}{GU^{s}_{ac,l}{}^2} \tag{22}$$

$$P^d_{dc,h} = P^{s,ref}_{dc,h} - \frac{rP^{s,ref2}_{dc,h}}{U^{s}_{dc,h}{}^2} \tag{23}$$

$$P^w_{ac,slack} = -\sum_{l=1}^{L} P^w_{ac,l} - \sum_{h=1}^{H} P^d_{dc,h} + P_{loss} \tag{24}$$

$$P^s_{ac,slack} = P^w_{ac,slack} + \frac{P^{w}_{ac,slack}{}^2}{GU^{ref2}_d} \tag{25}$$

where the subscript l represents the non-slack AC port of PET, the subscript h represents the non-slack DC port of PET, the subscript $slack$ represents the slack port of PET, L is the number of non-slack AC ports of PET, and H is the number of DC ports of PET.

(7) Determine the initial value of the control variable of the slack port. The calculation formulas are as follows:

$$\theta_{slack,0} = arctan(\frac{P^s_{ac,slack}}{-BU^{s}_{ac}{}^2 - Q^{s,ref}_{ac,slack}}) \tag{26}$$

$$m_{slack,0} = -\sqrt{2}\frac{P^s_{ac,slack}}{BU^{s,ref}_{ac,slack}U^{ref}_d sin(\theta_{slack,0})} \tag{27}$$

where $\theta_{slack,0}$ represents the initial value of the angle by which the voltage phase of the AC node connected to the slack port advances the phase of the voltage of VSC on the side of the slack port, and $m_{slack,0}$ represents the initial value of the modulation ratio of VSC on the slack port side.

(8) Calculate the power flow on the slack port side. If the power flow calculation converges, continue step (9); otherwise, return to step (3).

(9) Update the injected power of the network node connected to the slack port.

(10) Calculate the power flow of the subsystem connected to the slack port. If the power flow calculation converges, continue step (10); otherwise, return to step (3).

(11) Obtain the injected power of the network node connected to the slack port. If the power variations at all slack ports are within the required range, the power flow calculation results of the whole system converge and turn to step (12). Otherwise, update the AC node voltage connected to the relaxation port and then return to step (7).

(12) The process ends.

The process of the AC/DC hybrid alternating iterative power flow algorithm is shown in Figure 7.

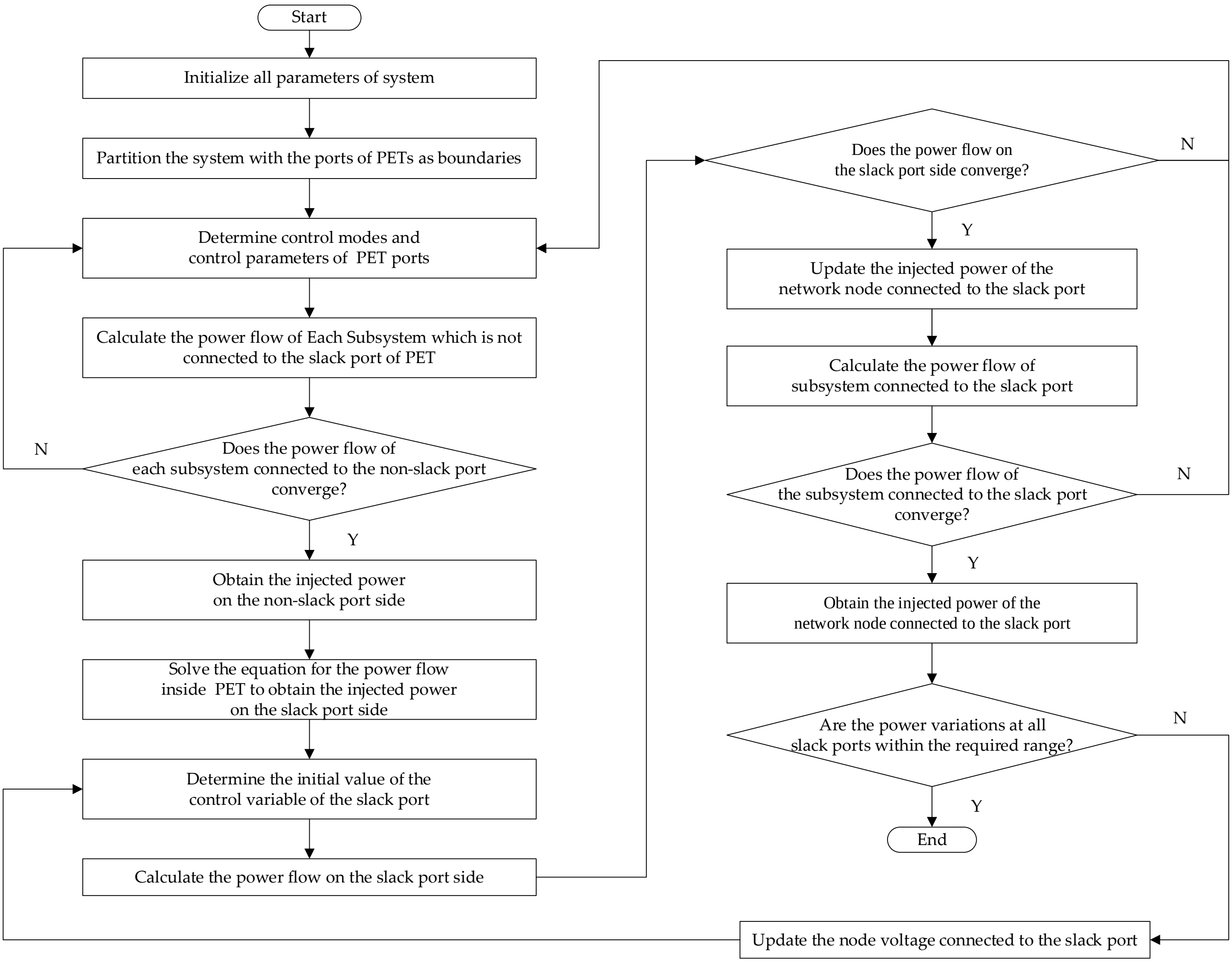

Figure 7. A flowchart of the power flow calculation process for AC/DC hybrid distribution networks with PETs.

5. Example Analysis

5.1. Example Construction and Parameter Setting

The analysis and solution process of the algorithm in this paper is based on the Windows11 operating system and Matlab R2020a numerical calculation platform on a laptop with an Intel Core i5-12500H (2.50 GHz) processor and 16 GB memory (Manufacturer: Honor Device Co., Ltd., Shenzhen, China). To verify the computational effectiveness of the power flow calculation method proposed in this paper, a ring AC/DC hybrid distribution network with PETs is used as an example for calculation and analysis. The system topology is shown in Figure 8. The numbers 1 to 40 in Figure 8 represent the node identifiers of the network topology, while D1 to D7 correspond to the respective ports of PETs. The AC distribution network of this algorithm is a modified IEEE33-bus system, where node 3 of the original system is changed to a four-port PET and a three-port PET is connected at the end of the network making the radial topology into a ring topology. The topology of the DC distribution network is selected from the reference [25], which is coupled with the AC distribution network through DC ports of two PETs. The total loads of distribution network are 8799.26 kW and 4847.32 kVar.

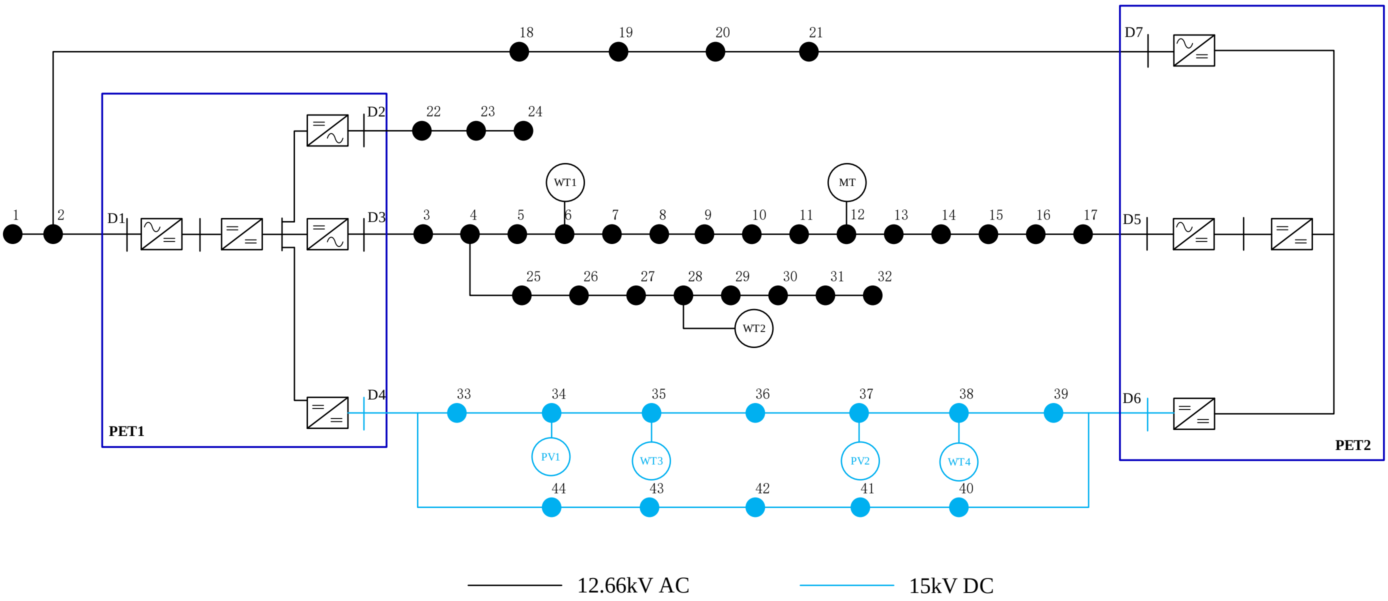

Figure 8. Improved IEEE 33-bus system connected to the DC system.

The rated voltage level of the AC system is 12.66 KV. The rated voltage level of the DC system is 15 KV. There are three DGs in the AC distribution network. Nodes 6 and 28 are connected to doubly fed asynchronous wind turbines, with a rated power of 400 kW and a power factor of 0.9. Node 12 is connected to the micro gas turbine, with a rated power of 500 kW. There are four DGs in the DC distribution network. Nodes 34 and 37 are connected to photovoltaic (PV) power sources with a rated power of 150 kW. Nodes 35 and 38 are connected to DC wind turbines, with a rated power of 200 kW. Gas turbines are controllable DGs, while wind turbines and photovoltaic power sources are uncontrollable DGs [26].

The capacity of both PETs is set to 5 MVA. To facilitate the analysis and comparison, the parameters of the AC/DC converters of two PETs are set identically, with the impedance parameter R set to 0.1 Ω and X set to 0.314 Ω [27]. Each PET has a static active power loss of 100 kW, and each AC port can provide reactive power compensation of up to 500 kVar. The allowable range of the inner DC bus voltage of PET is set to $1.8 < U_d < 2.2$ [28].

Taking the ports of PETs as the boundary, the AC/DC hybrid distribution network is divided into four zones, and the partitioning results are shown in Figure 9 and Table 2.

Table 2. The partition of the AC/DC hybrid distribution network.

Zone of Network	Nodes Included	Ports Connected
AC subnetwork 1	1, 2, 18~21	D1, D7
AC subnetwork 2	22, 23, 24	D2
AC subnetwork 3	3~17, 25~32	D3, D5
DC subnetwork	33~44	D4, D6

As shown in Table 2, AC subnetwork 1, AC subnetwork 2, AC subnetwork 3, and the DC network are four zones of 44-node AC/DC hybrid distribution network. AC subnetwork 1 connected to the port D1 of PET1 and the port D7 of PET2 includes nodes 1, 2, and 18~21. AC subnetwork 2 connected to the port D2 of PET1 includes nodes 22, 23, and 24. AC subnetwork 3 connected to the port D3 of PET1 and the port D5 of PET2 includes nodes 3~17 and 25~32. The DC subnetwork connected to the port D4 of PET1 and the port D6 of PET2 includes nodes 33~34. Figure 9 offers an intuitive understanding of the characteristic of subnetworks. AC subnetwork 1 is an active network, and its connected ports D1 and D7 both operate in Mode 2. AC subnetwork 2 is a passive network, and its connected port D2 operates in Mode 3. AC subnetwork 3 is an active network, and its connected ports D3 and D5 both operate in Mode 1. The DC network is a passive network, and its connected ports D4 and D6 operate in Mode 4 and Mode 5, respectively. Control modes of two PETs are shown in Table 3.

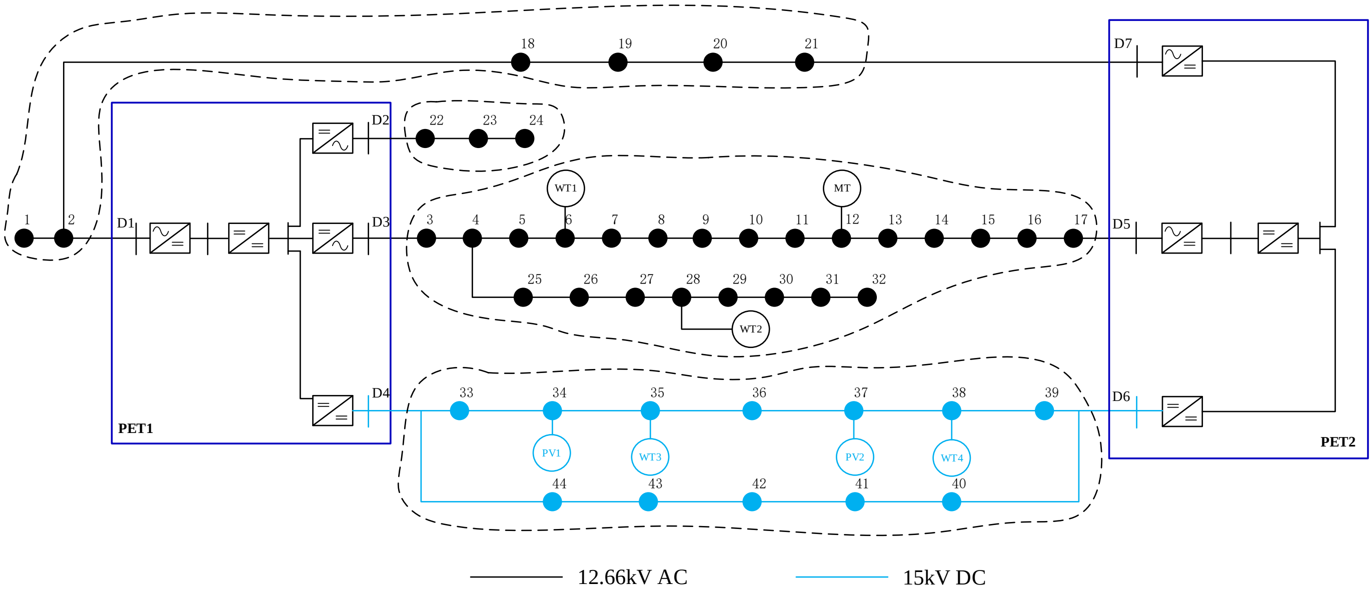

Figure 9. Partition results.

Table 3. Control modes of two PETs.

PET Number	Port Number	Control Modes
PET1	D1	Mode 2 : Constant U_d and Q_{ac}
	D2	Mode 3 : Constant U_{ac}^s and θ_{ac}^s
	D3	Mode 1 : Constant P_{ac} and Q_{ac}
	D4	Mode 4 : Constant P_{dc}^s
PET2	D5	Mode 1 : Constant P_{ac} and Q_{ac}
	D6	Mode 5 : Constant U_{dc}
	D7	Mode 2 : Constant U_d and Q_{ac}

The micro gas turbine MT can play a role in balancing the power of the network, so node 12, which is the access position of the MT, is considered as the balancing node of the AC subnetwork 3. According to the control mode of each port of PET in Table 3, the balancing nodes of the remaining subnetworks are set as node 1, node 22, and node 33, respectively.

5.2. Analysis of Power Flow Calculation Results

The basic capacity of the system is 10 MVA. The convergence accuracy of the proposed power flow calculation method is set to be 1×10^{-6} p.u., and the flow into the PET port is regarded as the positive direction of power. The active outputs of doubly fed asynchronous wind turbines connected to nodes 6 and 28 are both 200 kW, and the reactive outputs are both 96 kVar. The PV outputs of nodes 34 and 37 are both 80 kW, and the outputs of DC wind turbines connected to nodes 35 and 38 are both 100 kW. Parameter settings of two PETs are shown in Table 4.

Table 4. Parameter setting of two PETs.

Port Number	P_{ac}/P_{dc} (p.u.)	Q_{ac} (p.u.)	U_{ac}/U_{dc} (p.u.)	θ_{ac} (°)	U_d (p.u.)
D1	/	0	/	/	2.0
D2	/	/	0.9990	0	/
D3	−0.1550	−0.05	/	/	/
D4	/	/	0.9999	/	/
D5	−0.0020	−0.05	/	/	/
D6	0.020	/	/	/	/
D7	/	−0.020	/	/	2.0

Using the power flow calculation method proposed in this paper, the calculation results of two PETs are shown in Figures 10–12 and Table 5.

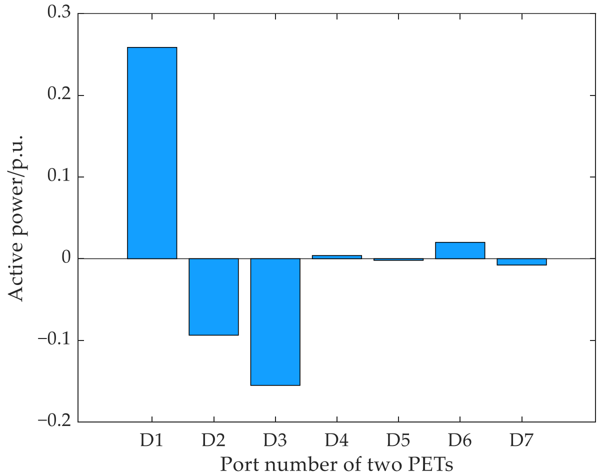

Figure 10. Active power of all ports of two PETs.

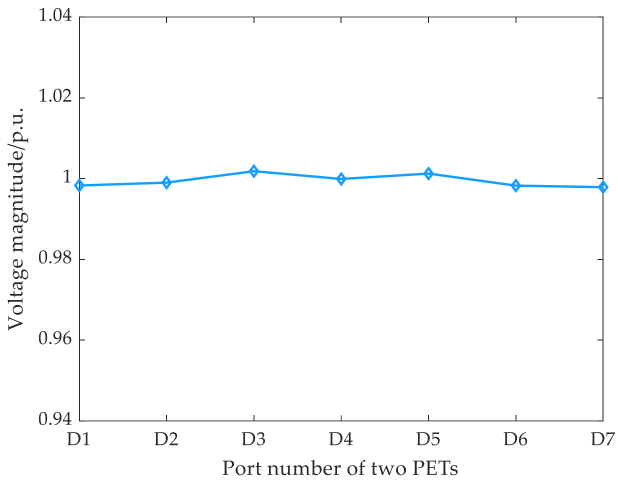

Figure 11. Voltage magnitude of all ports of two PETs.

According to Table 5, it is observed that all port variables of two PETs are within the permissible range, thus proving the effectiveness of the control scheme for multiple PETs in the AC/DC hybrid network and the hybrid alternating iteration method for solving the power flow of the ring AC/DC hybrid network with multiple PETs.

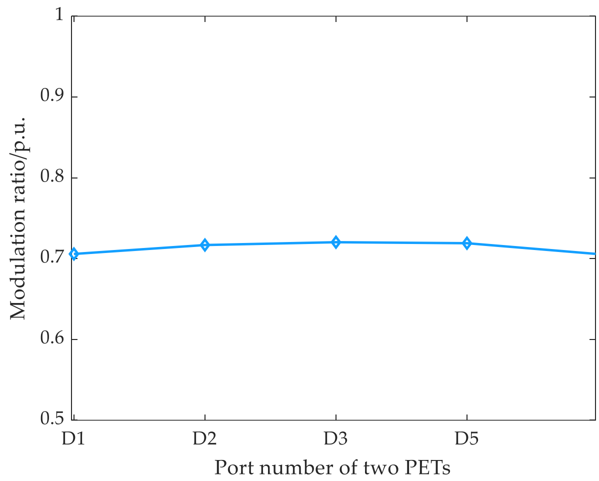

Figure 12. Modulation ratio of AC ports of two PETs.

Table 5. Power flow calculation results of two PETs.

Port Number	P_{ac}/P_{dc} (p.u.)	Q_{ac} (p.u.)	U_{ac}/U_{dc} (p.u.)	m (p.u.)	θ (°)
D1	0.2585	0	0.9983	0.7058	0.0291
D2	−0.0936	−0.0455	0.9990	0.7168	−1.6634
D3	−0.1550	−0.0500	1.00318	0.7203	−2.7335
D4	−0.0039	/	0.9999	/	/
D5	−0.0020	−0.0500	1.0012	0.7191	−0.0353
D6	0.0200	/	0.9983	/	/
D7	−0.0078	−0.0200	0.9979	0.7056	−0.0002

5.3. Analysis of the Impact of the Output Mutation of DGs

To verify the accuracy of the algorithm proposed and the ability of PET to regulate the output mutation of DGs, the following three cases are established:

Case 1: The examples in Section 5.2 serve as a control group without any changes. The active outputs of doubly fed asynchronous wind turbines connected to nodes 6 and 28 are both 200 kW, and the reactive outputs are both 96.86 kVar. The PV outputs of nodes 34 and 37 are both 80 kW, and the outputs of DC wind turbines connected to nodes 35 and 38 are both 100 kW.

Case 2: Simulate a night with sufficient wind power, set the wind turbine at rated output, and set the PV output to zero. The active outputs of doubly fed asynchronous wind turbines connected to nodes 6 and 28 are both 400 kW, and the reactive outputs are both 193.7 kVar. The PV outputs of nodes 34 and 37 are both 0 kW, and the outputs of DC wind turbines connected to nodes 35 and 38 are both 200 kW.

Case 3: Simulate extreme output conditions and set the wind turbine and the PV at a rated output. The active outputs of doubly fed asynchronous wind turbines connected to nodes 6 and 28 are both 400 kW, and the reactive outputs are both 193.7 kVar. The PV outputs of nodes 34 and 37 are both 150 kW, and the outputs of DC wind turbines connected to nodes 35 and 38 are both 200 kW.

Outputs of PVs and WTs in three cases are shown in Figure 13.

Based on the hybrid alternating iteration method proposed in this paper, voltage magnitudes of all nodes in the AC/DC hybrid distribution network with PETs in three cases are shown in Figure 14. In the AC distribution network part, the bus voltage distribution of each branch roughly shows a gradual downward trend towards the end of the network. Because nodes 6 and 28 are connected to DGs, the voltage rise phenomenon occurs. In the ring DC distribution network part, the voltage of each node is approximately the same.

The above voltage distribution characteristics are consistent with the voltage distribution law of the AC/DC hybrid distribution network.

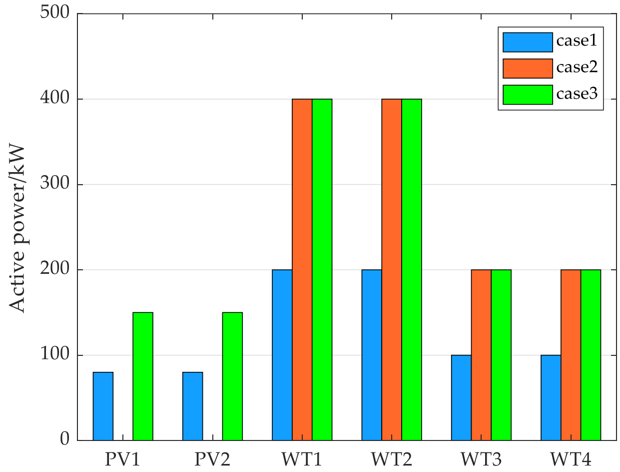

Figure 13. Outputs of PVs and WTs in three cases.

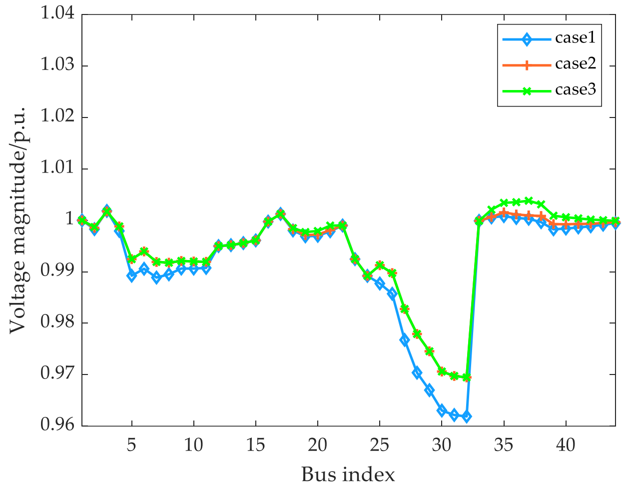

Figure 14. Comparisons of the bus voltage magnitudes between three cases.

The allowable offset range of the bus voltage magnitude is 0.95~1.05 p.u. Figure 14 shows that the voltage magnitudes of all the nodes are located at more than 0.96 p.u., which indicates the accuracy of the hybrid alternating iteration method.

Taking the bus voltage magnitudes of case 1 as the benchmark, the bus voltage magnitudes offset distribution is shown in Figure 15, which shows that the maximum value of bus voltage magnitudes offset is 0.789%. Consequently, PET possesses the capacity to reduce the impact of fluctuations in DGs on the operation results and has a supportive effect on the bus voltages.

The active power of all nodes in the AC/DC hybrid distribution network with PETs in three cases is shown in Figure 16. It can be observed that the control scheme of the two PETs is consistent with the power supply and demand characteristics of each region. AC subnetwork 1 connected to the system and the DC subnetwork rich in DGs continuously transmit power to AC subnetwork 3 with a heavy load to meet the power demand of area 3. With the increase in DG outputs in AC subnetwork 3, the active power absorbed by D1 connected to AC subnetwork 1 decreases, the active power output of D2 and D3 connected to region 3 increases, and the active power absorbed by D4 and D6 connected to the DC subnetwork increases. In conclusion, grid voltages remain stable during sudden changes in the output of distributed power sources due to the ability of PET to regulate the power dynamically.

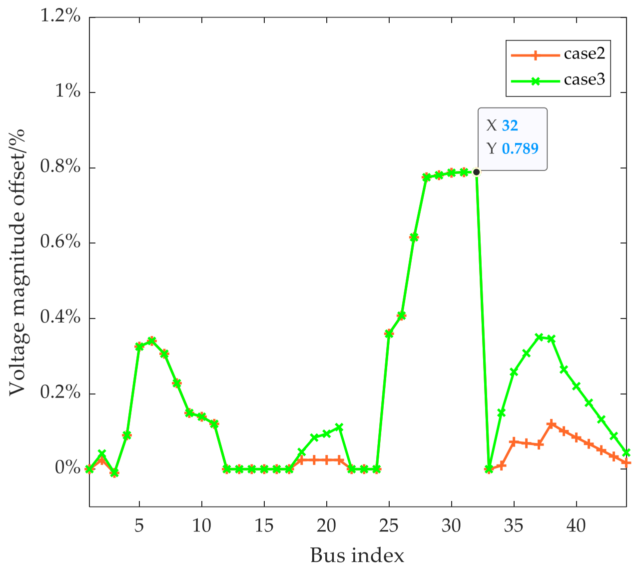

Figure 15. Bus voltage offset distribution of case 2 and case 3.

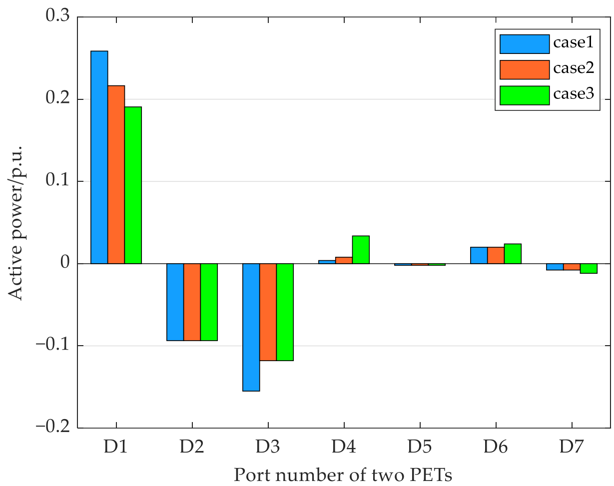

Figure 16. Comparisons of the active power of all ports of two PETs between three cases.

6. Discussion

The proposed hybrid alternating iterative power flow algorithm represents a significant advancement in power flow analysis for AC/DC hybrid networks with multiple PETs. Compared to existing methods, the algorithm addresses key challenges in handling complex ring topologies and tightly coupled AC/DC systems.

Traditional power flow calculation methods, such as the NR method and the Zbus Gaussian method, have shown limitations in dealing with hybrid networks. NR is well-suited for nonlinear AC network calculations but can be computationally intensive, particularly for large-scale systems. The Zbus Gaussian method, on the other hand, is efficient for linear systems such as DC networks but lacks the capability to handle the nonlinearities of AC/DC interactions effectively. By combining these methods in a hybrid iterative framework, the proposed algorithm leverages their respective strengths while mitigating their weaknesses. The validation of the proposed algorithm on a 44-node network demonstrates its adaptability and accuracy. Figure 14 shows that the voltage magnitudes of all nodes ranges from 0.95 p.u. to 1.05 p.u., and Figure 16 shows that the maximum value of bus voltage magnitudes offset is 0.789%, which further indicates the accuracy of the hybrid alternating iteration method.

Several existing methods have been proposed for power flow calculations in AC/DC hybrid networks, each with unique features and limitations. Reference [23] introduces iterative methods focusing on energy router models. These methods effectively enhance the coupling between AC and DC subsystems but may face computational challenges in highly interconnected ring topologies. In contrast, the proposed algorithm leverages the strengths of NR for non-linear AC systems and the Zbus Gaussian method for linear DC systems, providing a more balanced approach for precision and efficiency. Reference [29] explores the coupling dynamics in flexible AC/DC interconnects. These models provide valuable insights into the system dynamics, but are mainly for radial or lightly meshed networks, and the AC and DC networks are not coupled via PET. The proposed algorithm extends these capabilities to deal with ring networks with PETs, ensuring convergence and stability in complex topologies.

7. Conclusions

This study proposes a hybrid alternating iterative power flow calculation method for AC/DC hybrid distribution networks with multiple power electronic transformers (PETs). The primary focus of this work is to address the challenges posed by ring network topologies and the presence of multiple PETs, which are inadequately handled by traditional power flow methods. Through the integration of the NR method for the AC network and the Zbus Gauss method for the DC network, the proposed algorithm achieves a balance between computational efficiency and precision. Simulation results on a 44-node test network demonstrate the method's capability to handle complex AC/DC hybrid systems, with improved convergence and robustness.

This paper contributes to the theoretical advancement of power flow modeling for hybrid systems while providing practical methodologies that can support the future development of smart grids and renewable energy integration. The main contributions are described in the following two aspects:

(1) Theoretical contributions: This research extends the existing body of knowledge by developing a hybrid alternating iteration algorithm that combines the NR method and Zbus Gaussian method. This innovation enhances the theoretical understanding of hybrid AC/DC interactions and provides a scalable method suitable for networks with diverse topological and operational complexities.
(2) Practical contributions: The proposed algorithm ensures compatibility with existing commercial software tools, making it readily deployable for industry applications. Moreover, the method's ability to handle PET-containing systems positions it as a valuable tool for future grid planning and operational optimization in smart grids and renewable energy integration.

Despite its advantages, the current study relies solely on simulation-based validation. Experimental validation on a physical testbed would provide further confidence in the method's practical applicability. Additionally, while the algorithm is computationally efficient for medium-scale systems, future studies could explore enhancements such as parallel processing or machine learning integration to optimize performance for ultra-large networks. Therefore, further research work is essential, and future work priorities include:

(1) Experimental validation: developing a physical experimental platform to validate the proposed algorithm in real-world scenarios, particularly for large-scale networks with dynamic operational conditions.
(2) Algorithm scalability: extending the method to accommodate ultra-large networks with thousands of nodes, while maintaining computational efficiency. Techniques

such as parallel processing or machine learning-based convergence acceleration could be explored.

(3) Integration with advanced technologies: investigating the integration of neural networks and heuristic optimizers to enhance the adaptability and decision-making capabilities of the power flow model. These technologies could further improve computational speed and real-time performance in dynamic environments.
(4) Dynamic and fault analysis: expanding the method to address dynamic behaviors and fault conditions in AC/DC hybrid networks, ensuring its robustness under transient scenarios.
(5) Economic and environmental considerations: incorporating cost and environmental factors into the power flow model to support multi-objective optimization, aligning with the goals of modern sustainable energy systems.

By addressing these areas, the proposed method can evolve into a more comprehensive tool for power system analysis and operation, paving the way for smarter, more resilient, and sustainable distribution networks.

Author Contributions: Conceptualization, Z.Z., C.H., X.M. and W.C.; methodology, Z.Z., C.H. and X.M.; software, Z.Z., C.H., W.C., Y.H. and D.P.; validation, Z.Z., C.H., M.W. and D.P.; formal analysis, Z.Z., C.H., X.M., W.C., Y.H., M.W. and D.P.; investigation, Z.Z., C.H., X.M., W.C. and Y.H.; resources, D.P.; data curation, Z.Z., X.M. and M.W.; writing—original draft preparation, D.P.; writing—review and editing, M.W.; supervision, Z.Z. All authors have read and agreed to the published version of the manuscript.

Funding: This research was funded by the project "Research on State Estimation of AC/DC Hybrid Distribution Network with Power Electronic Transformer Based on Multi-source Measurement Data Fusion (520934230009)" from State Grid Shanghai Electric Power Company Qingpu Power Supply Company.

Data Availability Statement: Data are unavailable due to privacy reasons.

Conflicts of Interest: Authors Zhen Zheng, Chenhong Huang, Xiaoli Ma, Wenwen Chen and Yinan Huang are employed by the State Grid Shanghai Electric Power Company Qingpu Power Supply Company. The remaining authors declare that the research was conducted in the absence of any commercial or financial relationships that could be construed as a potential conflict of interest.

References

1. Li, K.; Zhao, Z.; Yuan, L.; Gao, C.; Wen, W.; You, X. Overview on Research of Multi-port Power Electronic Transformer Oriented for AC/DC Hybrid Distribution Grid. *High Voltage Eng.* **2021**, *47*, 1233–1250.
2. Chen, H.; Chen, J.; Duan, X. Study on Power Flow Calculation of Distribution System with DGs. *Autom. Electr. Power Syst.* **2006**, *30*, 35–40.
3. Zhao, D.; Jia, Y.; Ren, C.; Zhang, B. Unified Control Strategy of AC/DC Bus Voltage in Hybrid Microgrid Based on Bidirectional Interfacing Converter. *Power Syst. Technol.* **2021**, *45*, 3105–3114. [CrossRef]
4. Li, F.; Qin, W.; Ren, C.; Wang, Q.; Han, X.; Wang, J. Virtual Synchronous Motor Control Strategy for Interfacing Converter in Hybrid AC/DC Micro-grid. *Proc. CSEE* **2019**, *39*, 3776–3788.
5. Salomonsson, D.; Sannino, A. Low-Voltage DC Distribution System for Commercial Power Systems with Sensitive Electronic Loads. *IEEE Trans. Power Deliv.* **2007**, *22*, 1620–1627. [CrossRef]
6. Barnes, M.; Kondoh, J.; Asano, H.; Oyarzabal, J.; Ventakaramanan, G.; Lasseter, R.; Hatziargyriou, N. Real-World MicroGrids-An Overview. In Proceedings of the IEEE International Conference on System of Systems Engineering, San Antonio, DE, USA, 16–18 April 2007.
7. Boroyevich, D.; Cvetković, I.; Dong, D.; Burgos, R.; Wang, F.; Lee, F.; Hatziargyriou, N. Future Electronic Power Distribution Systems a Contemplative View. In Proceedings of the 12th International Conference on Optimization of Electrical and Electronic Equipment, Brasov, Romania, 20–22 May 2010.

8. Jakka, V.; Shukla, A. Integration of AC and DC Sources Using Multi-source Fed Power Electronic Transformer (MSF-PET) for Modern Power Distribution System Applications. In Proceedings of the 18th European Conference on Power Electronics and Applications, Karlsruhe, Germany, 5–9 September 2016.
9. Zhu, J.; Li, F.; Yu, L.; Li, X.; Wang, C. Autonomous Power Mutual Support Control for AC/DC Microgrid Interconnected by Solid State Transformer. *Power Syst. Technol.* **2023**, *47*, 284–295.
10. Pu, T.; Li, Y.; Chen, N.; Sun, Y.; Mu, Y.; Dong, L.; Kong, L. Key Technology and Research Framework for Optimal Operation Control of Hybrid AC/DC System Based on Power Electronic Transformer. *Power Syst. Technol.* **2018**, *42*, 2752–2759.
11. Kang, M.; Enjeti, P.; Pitel, I. Analysis and design of electronic transformers for electric power distribution system. *IEEE Trans. Power Electron.* **1999**, *14*, 1133–1141. [CrossRef]
12. Jin, G.; Shi, C.; Li, G.; Pan, D.; Liu, Z. Power Flow Calculation of an AC-DC Hybrid Distribution Network based on A Network Matrix. *Power Syst. Prot. Control.* **2020**, *48*, 52–61.
13. Lei, J.; An, T.; Du, Z.; Yuan, Z. A Unified AC/DC Power Flow Algorithm with DC Distribution. *Proc. CSEE* **2016**, *36*, 911–918.
14. Lei, J.; An, T.; Du, Z.; Yuan, Z. A General Unified AC/DC Power Flow Algorithm With MTDC. *IEEE Trans. Power Syst.* **2017**, *32*, 2837–2846. [CrossRef]
15. Chai, R.; Zhang, B.; Dou, J.; Hao, Z.; Zheng, T. Unified Power Flow Algorithm Based on the NR Method for Hybrid AC/DC Grids Incorporating VSCs. *IEEE Trans. Power Syst.* **2016**, *31*, 4310–4318. [CrossRef]
16. Chai, R.; Zhang, B.; Bo, Z. Alternating Iterative Power Flow Algorithm for Hybrid AC/DC Networks Containing DC Grid Based on Voltage Source Converter. *Autom. Electr. Power Syst.* **2015**, *39*, 7–13.
17. Wu, Z.; Yin, Z.; Tang, X. An AC/DC Decoupled Hybrid Power Flow Algorithm for Hybrid Power System. *Proc. CSEE* **2016**, *36*, 937–944.
18. Chen, Y.; Hao, Q.; Zhang, J. Dynamic Flow Algorithm for Hybrid AC/DC Networks With VSC-HVDC. *Power Syst. Technol.* **2016**, *40*, 1025–1029.
19. Li, Z.; Gao, F.; Zhao, C.; Wang, Z.; Zhang, H.; Wang, P.; Li, Y. Research Review of Power Electronic Transformer Technologies. *Proc. CSEE* **2018**, *38*, 1274–1289.
20. Miao, J.; Zhang, N.; Kang, C. Analysis on the Influence of Energy Router on the Optimal Operation of Distribution Network. *Proc. CSEE* **2017**, *37*, 2832–2839.
21. Huang, L.; Zong, C.; Yang, X.; Chen, W.; Zhu, Y.; Bi, K. Power Flow Calculation of Distribution Network with Multiple Energy Routers. *IEEE Access* **2021**, *9*, 23489–23497. [CrossRef]
22. Zhu, Y.; Wu, H.; Zhang, Z.; Zong, C.; Bi, K.; Xu, D. Power Flow Calculation of AC-DC Hybrid Distribution Network with Energy Routers. *Electr. Power Eng. Technol.* **2024**, *43*, 136–145.
23. Zhao, J.; Dou, J.; Wu, Y.; Xia, H.; Duan, Q.; Dong, X.; Zhang, Y. A Method for Power Flow Calculation in AC/DC Hybrid Distribution Networks Considering the Electric Energy Routers Based on an Alternating Iterative approach. *Electronics* **2024**, *13*, 3384. [CrossRef]
24. Peng, K.; Zhang, X.; Chen, Y. Power flow calculation algorithm for AC-DC hybrid distribution network with multi-terminal flexible interconnection. *Electr. Power Autom. Equip.* **2017**, *37*, 22–27.
25. Ma, X.; Gup, R.; Liu, J.; Fang, C.; Zhu, P.; Zhang, Y. State Estimation for Three-phase Unbalanced AC/DC Distribution Network. *Autom. Electr. Power Syst.* **2019**, *43*, 65–71.
26. Zhang, T.; Mu, Y.; Jia, H.; Wang, X.; Pu, T. Stochastic Operation Optimization for AC/DC Distribution Network with Power Electronic Transformer. *Power Syst. Technol.* **2022**, *46*, 860–869.
27. Cao, F.; Liu, C.; Li, X. Alternative Iteration Algorithm for Power Flow of Distribution Network with Power Electronic Transformer. *Adv. Technol. Electr. Eng. Energy* **2018**, *37*, 41–50.
28. Zheng, C.; Zhou, X.; Li, R.; Sheng, C. Study on the Steady Characteristic and Algorithm of Power Flow for VSC-HDC. *Proc. CSEE* **2005**, *25*, 4–8.
29. Zhang, Y.; Zhang, J.; Liu, G. Hybrid Power Flow Calculation of AC-DC Flexible Interconnected System in Distribution Network, In Proceedings of the 2021 IEEE Sustainable Power and Energy Conference, Nanjing, China, 23–25 December 2021.